

Coarsening dynamics in one dimension: the phase diffusion equation and its numerical implementation

Matteo Nicoli,¹ Chaouqi Misbah,² and Paolo Politi³

¹*Physique de la Matière Condensée, École Polytechnique, CNRS, Palaiseau, F-91128 France**

²*Univ. Grenoble 1 / CNRS, LIPhy UMR 5588, Grenoble, F-38041, France*

³*Istituto dei Sistemi Complessi, Consiglio Nazionale Delle Ricerche, via Madonna Del Piano 10, I-50019 Sesto Fiorentino, Italy*

Many nonlinear partial differential equations (PDEs) display a coarsening dynamics, i.e., an emerging pattern whose typical length scale L increases with time. The so-called coarsening exponent n characterizes the time dependence of the scale of the pattern, $L(t) \approx t^n$, and coarsening dynamics can be described by a diffusion equation for the phase of the pattern. By means of a multiscale analysis we are able to find the analytical expression of such diffusion equations. Here, we propose a recipe to implement numerically the determination of $D(\lambda)$, the phase diffusion coefficient, as a function of the wavelength λ of the base steady state $u_0(x)$. D carries all information about coarsening dynamics and, through the relation $|D(L)| \simeq L^2/t$, it allows us to determine the coarsening exponent. The main conceptual message is that the coarsening exponent is determined without solving a time-dependent equation, but only by inspecting the periodic steady-state solutions. This provides a much faster strategy than a forward time-dependent calculation. We discuss our method for several different PDEs, both conserved and not conserved.

I. INTRODUCTION

In this paper we will focus on the nonlinear dynamics of one-dimensional (1D) partial differential equations (PDEs), having the form [1]

$$\partial_t u = \mathcal{N}[u], \quad (1)$$

where \mathcal{N} is a general nonlinear operator, not depending explicitly on time t and space x and whose trivial solution $u \equiv 0$ has a linear stability spectrum whose modes of sufficiently small wave vector are unstable. More precisely, setting $u(x, t) = \bar{u} \exp(iqx + \omega t)$, and keeping only terms that are linear in \bar{u} , one obtains a dispersion relation relating ω to q . Two well-known dispersion relations [1] are,

$$\omega(q) = 1 - q^2 \quad \text{nonconserved models,} \quad (2a)$$

$$\omega(q) = q^2 - q^4 \quad \text{conserved models.} \quad (2b)$$

In both cases $\omega(q) > 0$ for $q < 1$. In other words, the trivial solution $u = 0$ is unstable for $q < 1$. This means that modes with arbitrary small wave numbers are unstable, and therefore, in principle, spatial structures with large wavelength can develop, so that the notion of coarsening makes sense. This implies that we exclude situations where there is a small q cut-off, that is, when there is a minimal wave number below which the trivial solution is stable. A typical example in this category is the Swift-Hohenberg equation [1], for which the dispersion relation takes the form $\omega(q) = \alpha + (q - 1)^2$, with α

a real parameter. This dispersion relation means that if $\alpha < 0$, then there is a minimal wave vector $q_{min} = 1 - \sqrt{\alpha}$ below which the trivial solution is stable. We do not expect in this case a structure with a wave number smaller than q_{min} to take place (no perpetual coarsening is *a priori* expected). While this statement complies with intuition, we must keep in mind that the stability evoked above follows from a linear analysis. Therefore, since the equations of interest are nonlinear, exceptions are not excluded [2]. Having in mind the occurrence of some exceptions, we will focus on systems having a linear dispersion relation of the form (2). This holds for many nonlinear PDEs. The most well-known equations are the Ginzburg-Landau (GL), the Cahn-Hilliard (CH), the Kuramoto-Sivashinsky (KS), and their variants or generalizations [1]. Equations of this class will be introduced and discussed in the next section.

Note that having unstable modes for small q as in (2) is not a sufficient condition. A prominent example is the KS equation, which shows spatiotemporal chaos, with wavelengths of constant average size being continuously destroyed and created. This is not surprising: the analysis of the linear stability spectrum does not univocally determines the nonlinear dynamics.

One important feature that we will discuss here is the determination of the branch of periodic steady-state solutions, which acquire a special status in our investigation of coarsening dynamics. This is *a priori* not obvious, since coarsening is a time-dependent process, but it has been shown before that stationary configurations of period λ , $u_0(x)$, play a major role in determining the type of nonlinear dynamics: for a certain class of nonlinear equations in one dimension, two of us have proven [3] that coarsening is possible if and only if the wavelength λ is an increasing function of the amplitude A of the solution $u_0(x)$, $\lambda'(A) > 0$. The presence of a maximum in the curve $\lambda(A)$ signals the phenomenon of interrupted

*Present address: Center for Interdisciplinary Research on Complex Systems, Department of Physics, Northeastern University, Boston, Massachusetts 02115, USA.

coarsening, while a decreasing $\lambda(A)$ signals no coarsening at all. Finally, for some equations such as KS, $\lambda(A)$ is not a single-value function and the curve displays a so-called turning point.

All these examples show that steady states contain important pieces of information. However, how is it possible that dynamics depends on stationary properties only? The answer to this question is contained in the concept of phase instability. For example, in one dimension, a steady-state periodic solution $u_0(x)$ has a wavelength (or wave number $q = 2\pi/\lambda$) λ such that $u_0(x + \lambda) = u_0(x)$. In this case the phase ϕ of the pattern is $\phi = qx$. However, a perturbation of the wavelength of the pattern (or equivalently a perturbation of the phase ϕ) may reveal instability (called phase instability), meaning that the wavelength will evolve in time, and if this is the case for any q , one may expect coarsening. A global shift of a periodic pattern in the x direction by a constant value x_0 is also a solution, i.e., $u_0(x + x_0) = u_0(x)$, owing to translational invariance (also called a Goldstone mode). This constant shift corresponds to a phase perturbation of infinite wavelength, and since it is a stationary solution, it has an infinite relaxation time towards the original solution $u_0(x)$. In other words, a large wavelength perturbation of the pattern is expected to have a large time scale. This entails that the most dangerous perturbations are those of long wavelengths of the phase of the pattern. To make this notion explicit, we introduce a small parameter ϵ expressing the fact that the phase modes of interest have a small spatial gradient, on the scale of the wavelength of the pattern. An appropriate way to deal with this question is to introduce a multiscale analysis: the fast spatial scale x (where the periodic profile of pattern varies on a scale of order unity) and a slow scale X (expressing the long wavelength perturbation of the phase of the pattern). The slow spatial scale, implies also a slow time scale (which can also be inferred from the above discussion about large relaxation times) T . It turns out that (see later) $X = \epsilon x$ and $T = \epsilon^2 t$.

If ϕ designates the actual phase of a pattern (not necessarily a periodic one, but some perturbed pattern), it will depend on space and time, e.g., because $u_0(x)$ is perturbed, and acquires a slow spatial and time dependence (i.e., it depends on X and T), which can be described by a phase diffusion equation (see next section), having the form

$$\partial_T \psi = D(q) \partial_{XX} \psi, \quad (3)$$

where ψ, X, T are suitably rescaled versions of ϕ, x, t , and the phase diffusion coefficient $D(q)$ only depends on properties of the steady-state solution of wavelength $\lambda = 2\pi/q$. A negative $D(q)$ signals a phase instability, i.e., coarsening. Other scenarios are possible [4]. Even if for several nonlinear equations it is feasible to obtain the analytical form of $D(q)$ in the limit of large λ , in the generic case it is not possible and we must determine it numerically, by computing the steady-state solution $u_0(x)$, from which we can state if the pattern is

stable (no coarsening), or unstable (coarsening). We will then show how the coarsening exponent (in the temporal power law) can be extracted from these considerations (i.e. without any time integration of the equations).

In this paper we start by briefly describing the multiscale method and apply it to several 1D PDEs, therefore extracting the quantities we need to determine $D(q)$ numerically. We will see that we need two functions: (i) $u_0(x)$, the stationary solution, which satisfies the equation $\mathcal{N}[u_0] = 0$, see Eq. (1), and (ii) $v_0(x)$, solution of the equation $\mathcal{L}^\dagger[v_0(x)] = 0$, where \mathcal{L} is the Frechét derivative of \mathcal{N} and \mathcal{L}^\dagger is its adjoint operator. We will show how it is possible to implement the numerical determination of such functions, therefore the determination of $D(q)$ and, finally, how we can get the coarsening exponent n , describing the time dependence of the typical scale, $L \approx t^n$, when coarsening is present. Particular attention will be devoted to the conserved Kuramoto-Sivashinsky (cKS) equation, because in such a case \mathcal{L} is not self-adjoint and special care must be devoted to the determination of $v_0(x)$.

II. FROM THE 1D NONLINEAR EQUATION TO THE PHASE DIFFUSION EQUATION

In this section we introduce all nonlinear equations we are going to discuss, we give a very brief sketch of the multiscale approach used to extract the phase diffusion equation, and we finally provide the expression of the phase diffusion coefficient D . In some cases, we just report existing results, but in the case of the cKS equation, we provide the original derivation of D , which will be seen to deserve special attention.

A. The models

Let us start by listing all equations of interest, the nonconserved first:

$$\partial_t u = u - u^3 + \partial_x^2 u \quad \text{GL equation,} \quad (4a)$$

$$\partial_t u = \frac{u}{(1 + u^2)^\alpha} + \partial_x^2 u, \quad \alpha \text{ models.} \quad (4b)$$

then their conservative counterparts:

$$\partial_t u = -\partial_x^2 [u - u^3 + \partial_x^2 u] \quad \text{CH equation,} \quad (5a)$$

$$\partial_t u = -\partial_x^2 \left[\frac{u}{(1 + u^2)^\alpha} + \partial_x^2 u \right] \quad \text{c}\alpha \text{ models.} \quad (5b)$$

and, finally, the conserved Kuramoto-Sivashinsky equation

$$\partial_t u = -\partial_x^2 [u - \tau \partial_x u + \partial_x^2 u - (\partial_x u)^2] \quad \text{cKS equation.} \quad (6)$$

GL and CH are classical equations [5] describing, e.g., phase separation processes for a scalar order parameter, either conserved (CH) or nonconserved (GL). The

$c\alpha$ model for $\alpha = 1$ first appeared in problems of crystal growth [6] and starting from that specific conserved model it has been natural to extend it [7] to $\alpha \neq 1$ and to the nonconserved case. Finally, the cKS equation appeared in the study of sand-ripple dynamics [8], then in step-bunching phenomena [9]. For $\tau = 0$ it also appears in the study of wandering crystalline steps [10, 11].

Equations (4) have the general form $\partial_t u = A(u) + \partial_x^2 u$ and their linear dispersion relation has the form (2a). All conservative equations, (5) and (6), have the form $\partial_t u = -\partial_x^2(\dots)$ and their linear dispersion relation is like (2b). For Eq. (6), that is true for $\tau = 0$ only. However, the τ term can be canceled out with a tilt transformation: $u \rightarrow u + \tau x/2$. We keep it here for sake of generality.

All previous models, conserved and nonconserved, display perpetual coarsening, because, as analyzed in the next subsection, they have a branch $u_0(x)$ of steady states whose $\lambda(A)$ characteristic is an increasing, diverging function.

B. The multiscale method and the phase diffusion equation

We are now going to discuss the multiscale method, with a focus on the cKS eq. This step has two motivations. First, the cKS equation is a completely non trivial equation, whose nonlinear dynamics has been studied only through direct numerical simulations or through a simplified particle model. We are not aware of analytical nonlinear studies. Second, its treatment with the multiscale approach is representative of the method, when the Frechét derivative is not self-adjoint.

The basic idea is to perturb a periodic steady state $u_0(x, \lambda) = u_0(x + \lambda, \lambda)$. First, we rescale x by introducing the phase $\phi = qx$, with $q = 2\pi/\lambda$, so that $u_0 = u_0(\phi, q)$. Next, we introduce slow space and time variables,

$$X = \epsilon x, \quad T = \epsilon^2 t, \quad (7)$$

and perturb u_0 so that q is now dependent on X and T . While x is the fast space variable, no fast time variable exists, since the base state $u_0(x)$ is a stationary state. The final step is to perform a multiple scale expansion method [12]. Identifying the slow phase $\psi(X, T) = \epsilon\phi(x, t)$, we can finally rewrite the space and time derivatives,

$$\partial_x = q\partial_\phi + \epsilon\partial_X = q\partial_\phi + \epsilon\psi_{XX}\partial_q, \quad (8a)$$

$$\partial_t = \epsilon\psi_T\partial_\phi. \quad (8b)$$

This is enough, along with the ϵ expansion of the solution, $u = u_0 + \epsilon u_1$, to perform a correct perturbative

analysis of Eq. (1). Using Eqs. (7)–(8), the general nonlinear equation (1) rewrites as

$$\begin{aligned} \epsilon(\partial_\phi u_0)\partial_T \psi &= (\mathcal{N}_0 + \epsilon\mathcal{N}_1)[u_0 + \epsilon u_1] \\ &= \mathcal{N}_0[u_0] + \epsilon\mathcal{L}_0[u_1] + \epsilon\mathcal{N}_1[u_0], \end{aligned} \quad (9)$$

where \mathcal{L}_0 is the functional, Frechét derivative of \mathcal{N}_0 . Since $\mathcal{N}_0[u_0]$ trivially vanishes, we are left with the first-order terms, which can be rearranged, so that the function u_0 appears in the source term, g , of the linear differential equation for u_1 ,

$$\mathcal{L}_0[u_1] = (\partial_\phi u_0)\partial_T \psi - \mathcal{N}_1[u_0] \equiv g. \quad (10)$$

According to the Fredholm alternative theorem [13], g must be orthogonal to the kernel of the adjoint operator, \mathcal{L}_0^\dagger . In conclusion, if

$$\mathcal{L}_0^\dagger[v_0] = 0, \quad (11)$$

then

$$\langle v_0, (\partial_\phi u_0)\partial_T \psi - \mathcal{N}_1[u_0] \rangle = 0. \quad (12)$$

In the next subsection we are going to see that Eq. (12) can be recast in the form of a phase diffusion equation,

$$\partial_T \psi = D(q) \partial_{XX} \psi, \quad (13)$$

where the phase diffusion coefficient, $D(q)$ is a nontrivial functional of u_0 and v_0 [14].

C. The phase diffusion coefficient

The application of the multiscale method to Eqs. (4) and (5) gives, respectively

$$D(q) = \frac{\partial_q \langle q (\partial_\phi u_0)^2 \rangle}{\langle (\partial_\phi u_0)^2 \rangle} \quad \text{nonconserved Eqs. (4), (14)}$$

and

$$D(q) = q^2 \frac{\partial_q \langle q (\partial_\phi u_0)^2 \rangle}{\langle u_0^2 \rangle} \quad \text{conserved Eqs. (5). (15)}$$

For the cKS equation (6), we give here below a few details for the derivation of $D(q)$. In that case, the operators appearing in Eqs. (9-12) are

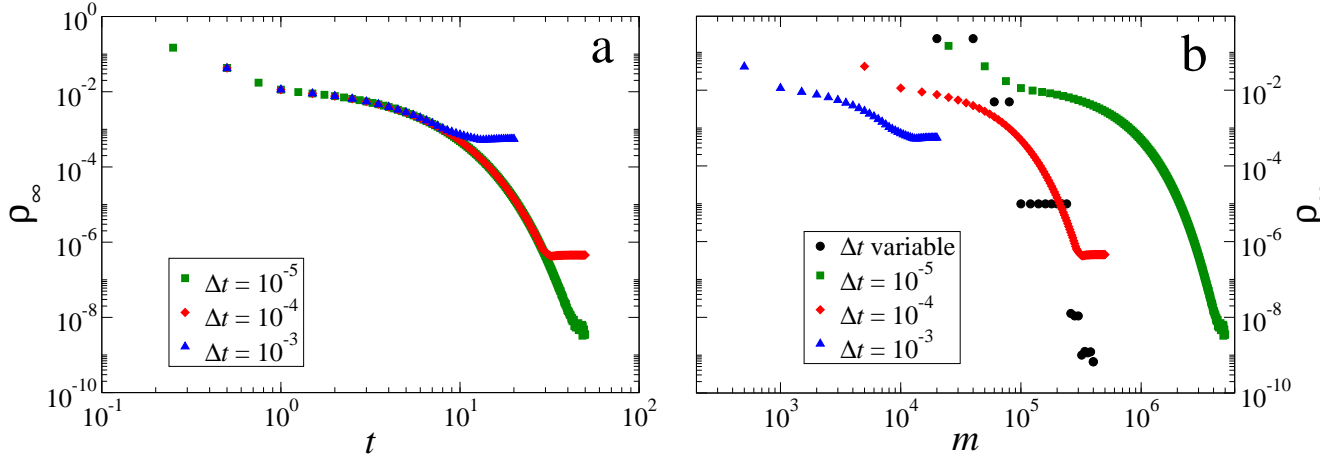


FIG. 1: (a) Evolution of the residue ρ_∞ of the Cahn-Hilliard equation (5a) as function of time for different values of Δt (reported in the legend). The initial condition is a sinusoid discretized by $N = 512$ points with $\lambda = 12.8$, corresponding to $q = 0.49087$. Note that for a fixed Δt the residue saturates at an asymptotic value, which depends on the magnitude of the time steps. (b) Evolution of ρ_∞ as function of the iteration step m for the same simulation condition of the left figure. The black points are the value of ρ_∞ for a numerical integration of Eq. (5a) with a variable time stepping. Starting from $\Delta t = 0.025$, the magnitude of Δt is reduced of a factor ten ($\delta t = 0.1$) every time the condition $\Delta \rho_\infty < 10^{-4}$ is verified. The numerical integration stops for $\rho_\infty < 10^{-9}$, value reached for $\Delta t = 2.5 \times 10^{-6}$. Note that the sudden improvements of the accuracy of the estimated solution u_0 are due to the reduction of Δt .

$$\mathcal{N}_0[u_0] = -q^2 \partial_\phi^2 \left[(1 - \tau q \partial_\phi + q^2 \partial_\phi^2) u_0 - q^2 (\partial_\phi u_0)^2 \right], \quad (16)$$

$$\mathcal{L}_0[u_1] = -q^2 \partial_\phi^2 \left[1 - \tau q \partial_\phi + q^2 \partial_\phi^2 - 2q^2 (\partial_\phi u_0) \partial_\phi \right] u_1, \quad (17)$$

$$\mathcal{N}_1[u_0] = -\psi_{XX} \left\{ q^2 \partial_\phi^2 [(2q \partial_q + 1) \partial_\phi u_0 - \tau \partial_q u_0 - 2q (\partial_\phi u_0) \partial_q u_0] \right\}, \quad (18)$$

$$\mathcal{L}_0^\dagger[v] = -q^2 \left\{ 1 + \tau q \partial_\phi + q^2 \partial_\phi^2 + 2q^2 [(\partial_\phi^2 u_0) + (\partial_\phi u_0) \partial_\phi] \right\} \partial_\phi^2 v. \quad (19)$$

Finally, from Eq. (12) we can determine the diffusion coefficient,

$$D(q) = -q^2 \langle \partial_\phi^2 v_0, (2q \partial_q + 1) \partial_\phi u_0 - \nu \partial_q u_0 - 2q (\partial_q u_0) \partial_\phi u_0 \rangle / \langle v_0, \partial_\phi u_0 \rangle. \quad (20)$$

When \mathcal{L}_0 is self-adjoint, as for Eqs. (4), translational invariance immediately provides the result $v_0 = \partial_\phi u_0$. For Eqs. (5), $\mathcal{L}_0^\dagger \neq \mathcal{L}_0$, but Eq. (11) can be easily solved analytically and v_0 is still related to u_0 through some differential operator. In all these cases, covering Eqs. (4a)–(5b), D can be expressed as a function of u_0 and its derivatives only, see Eqs. (14)–(15). Finally, there are cases where $\mathcal{L}_0^\dagger \neq \mathcal{L}_0$ and v_0 cannot be determined analytically. The cKS equation is a typical example. In the next section we discuss the most general implementation for a numerical determination of u_0, v_0 and D .

III. NUMERICAL IMPLEMENTATION

The numerical procedure we have developed to find the value of D for a given λ can be split in three parts: (i) The determination of the stationary solution u_0 by employing a pseudospectral algorithm (see Appendix A) and, only if required, a Newton-Raphson method to increase the accuracy of the output of our pseudospectral code. (ii) In the second step, the function v_0 is found by discretizing the adjoint \mathcal{L}_0^\dagger of the Frechét derivative of \mathcal{N}_0 with high order finite differences and finding the kernel of the sparse matrix M containing the coefficients of the discrete version of \mathcal{L}_0^\dagger . Clearly, we skip this step when we are able to obtain v_0 analytically. (iii) Lastly, the value of $D(\lambda)$ is computed with a standard numerical integration after the evaluation of the derivatives (in

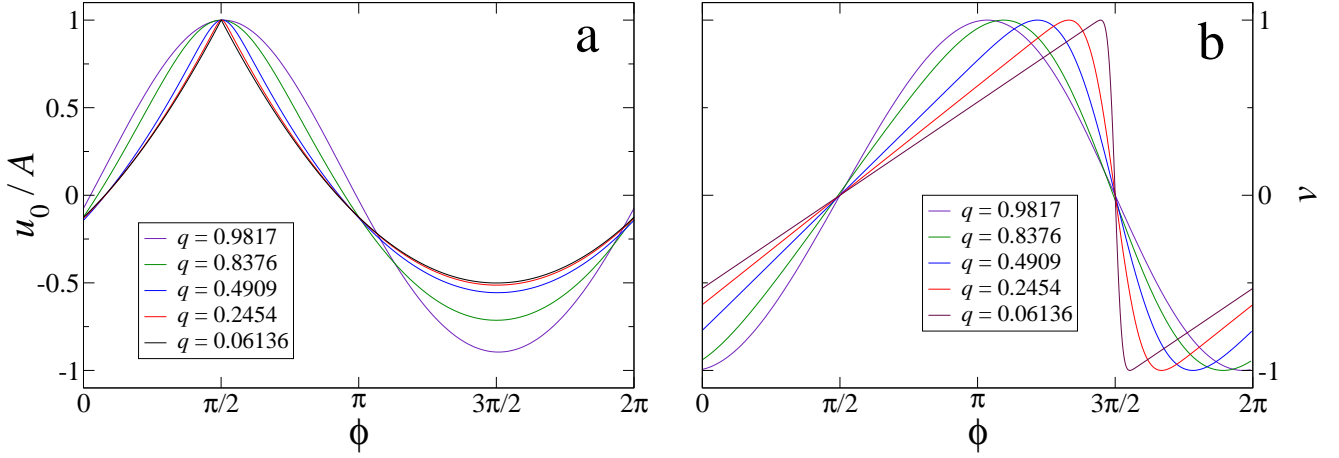


FIG. 2: (a) Normalized stationary solutions u_0 of equation (23) with $\tau = 0$ for different values of q . The differential operators are discretized in an uniform grid with $\Delta\phi = 0.025$. For visualization purposes we have chosen a normalization constant $A = \max |u(\phi)|$. (b) Solutions of the adjoint problem $\mathcal{L}_0^\dagger[v_0] = 0$, see Eq. (19), with $\tau = 0$. As for the left figure, the spatial discretization is $\Delta\phi = 0.025$.

ϕ and q space) of u_0 and, if necessary, v_0 (only for the cKS equation). These three steps are iterated for each λ and, finally, the coarsening exponent is estimated using the relation $|D| \sim L^2/t$.

A. Determination of the stationary solutions

The time-dependent problem (1) can be integrated very efficiently by using a pseudospectral algorithm. These methods are widely used for the integration of nonlinear PDEs because they combine the estimation of spatial derivatives in Fourier space with the calculation of nonlinear terms in real space, hence avoiding the computational overhead of the convolution step [15–18]. Pseudospectral methods mainly work in Fourier space and their strength resides in their high accuracy for smooth solutions.

It is convenient to restate the nonlinear problem (1) in $\phi \in [0, 2\pi]$ space, by replacing the derivatives ∂_x with $q\partial_\phi$. In this way, stationary solutions obtained at different values of q are mapped into the same interval so that they can be directly compared.

Every nonlinear PDE such as Eq. (1) can be divided into a linear operator ω , the dispersion relation, and a nonlinear operator N , such that in Fourier space Eq. (1) reads

$$\partial_t u_k(t) = \omega_k u_k(t) + N[u(t)]_k, \quad (21)$$

where $N[u]_k$ is the Fourier transform of the nonlinear part of the PDE, and the discrete wave vectors k belong to the interval $[-N/2, N/2]$, with the same $\Delta k = 1$ for every λ (here N is the number of points used to discretize the ϕ interval). Equation (21) is evaluated by using the *integrating factor* technique [15, 18]

and time stepped with a fourth-order Adams-Bashforth-Moulton predictor-corrector scheme (IFABM4) [19] (see Appendix A for the details of the numerical implementation). For a comparison between different pseudospectral algorithms see Ref. [20] and references therein.

The IFABM4 method has been used in this paper to study the time evolution of Eq. (1) and to characterize the coarsening exponent by measuring the mean wavelength of the emerging pattern, $L(t)$, as a function of time t . In order to obtain a reliable estimate of n , the function $L(t)$ must be averaged over several realizations, each one with a different initial condition.

Stationary solutions of nonlinear PDEs are normally found with specialized approaches that have better performances compared to any numerical integration of the dynamics of Eq. (1). Although point collocation or multi-grid methods [19] are less computationally expensive than our IFABM4 code, we decided to rely on the same algorithm to highlight the advantages of a strategy based on the the phase-diffusion equation. Moreover, even if it is well established that the integrating factor technique can lead to a wrong estimation of the fixed points of nonlinear ODEs [21] and more accurate algorithms have been already developed for ODEs [21] and PDEs [20], such as Eq. (1), a small modification of the IFABM4 algorithm allowed us to find the stationary solutions u_0 with a reasonable precision (enough for our purposes).

Starting from an initial guess function $u(x, 0)$, the dynamics of Eq. (21) leads to the closest stationary solution. Obviously this can happen only when at least one u_0 exists for the fixed value λ and for the chosen parameters (α, τ, \dots) considered during the integration of Eq. (21). The error committed in the estimation of the stationary

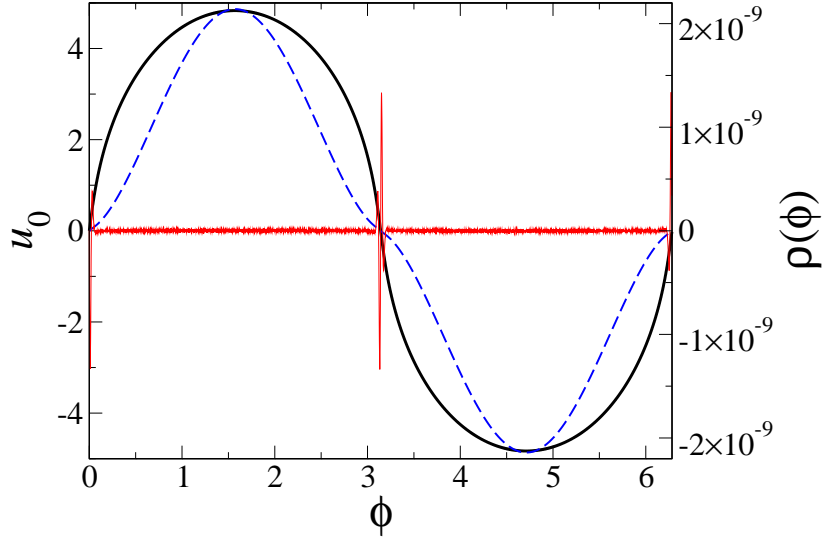


FIG. 3: Left vertical axis: Stationary solution u_0 (thick full line) of Eq. (4b) with $\alpha = 2$ and $\lambda = 102.4$, corresponding to $q = 0.061359$. The parameters of the IFABM4 algorithm are $N = 4096$, $\Delta t = 0.1$, $\delta t = 0.1$, $\Delta \rho_{min} = 10^{-4}$, and a stopping condition $\rho_\infty < 5 \times 10^{-9}$. Right vertical axis: residue $\rho(\phi)$ before (blue, thin line) and after (red, dashed line) the Newton-Raphson minimization.

solution is easily quantified by inspecting the residues

$$\begin{aligned} \rho(\phi) &= \mathcal{F}^{-1} [\omega_k u_k]_\phi + \mathcal{N}[u(\phi)], \\ \rho_\infty &= \max |\rho(\phi)|, \\ \rho_2 &= \int_0^{2\pi} d\phi \rho^2, \end{aligned} \quad (22)$$

during the numerical integration of the PDE. As shown in Fig. 1(a), for a fixed value of Δt we observe that ρ_∞ saturates at an asymptotic value depending on the magnitude of the time steps. Even if starting the numerical integration of Eq. (21) with a tiny Δt ensures a small asymptotic residue, this will increase enormously the computational cost required to find u_0 , therefore impairing the applicability of this method to many practical cases.

A possibility to overcome this trade-off between accuracy and computational effort arises when we take into account that here our goal is not to follow the real dynamics of Eq. (21) but rather to obtain a reliable estimate of its stationary solutions. The numerical convergence of $u(t)$ to u_0 can be increased by reducing dynamically the value of Δt . Actually, by monitoring the residue and its variation $\Delta \rho_\infty^m = |\rho_\infty^m - \rho_\infty^{m-m_c}| / \rho_\infty^m$ (here the superscript m stands for the discrete time) every predefined number of iteration steps m_c , we are able to sense when the dynamics of the PDE has reached the stationary state for a given Δt . In fact, a drop of $\Delta \rho_\infty^m$ below a given threshold $\Delta \rho_{min}$ means that the residual error cannot be diminished anymore, signaling that is the appropriate moment to reduce Δt by multiplying its value for a factor $\delta_t < 1$. After every reduction of the time step, the predictor-corrector scheme has to be warmed up by a method of equal accuracy, such as a fourth-order Runge-Kutta (see Appendix A for its numerical implementation). In gen-

eral, the values of $\Delta \rho_{min}$ and δ_t have to be inferred empirically for each problem: for our analysis, we have used $\Delta \rho_{min} = 10^{-4}$ and $\delta_t = 0.1$. Additionally, m_c must be a large number in order to limit the computational overhead required for the estimation of the residue and its variation. For one-dimensional problems a value of m_c between 10^3 and 10^4 is a reasonable choice. As an example, in Fig. 1(b) we report a comparison between the constant and the variable time stepping in case of the Cahn-Hilliard equation (5a).

In some cases the solution found by the pseudospectral algorithm is not accurate enough to ensure a good estimation of the coarsening law, through the evaluation of $D(q)$. This usually happens for large system sizes, so that the algorithm converges slowly, or when the variations of the stationary solution are extremely localized and the resolution of the numerical method is insufficient to resolve these jumps (spectral methods are not suitable to handle discontinuities like shocks). To improve the residue of u_0 we have employed a Newton-Raphson (NR) method applied to the finite difference discretization (in ϕ space) of the equation $\mathcal{N}[u] = 0$. To be more precise, in case of an operator \mathcal{N} that can be written as a second-order derivative of another nonlinear operator \mathcal{N}_r (that is $\mathcal{N}[u] = -\partial_x^2 \mathcal{N}_r[u]$) we have found the solutions of equation $\mathcal{N}_r[u] = 0$ and then subtracted to these functions their mean value $\langle u_0 \rangle$. In fact, these type of nonlinear operators are conservative so that the mean value of u is preserved by the dynamics of the equation, and, additionally, we can deal with an operator that is less stiff than the original one. Besides, it is sufficient to find the stationary solution of the GL equation (4a) to compute the phase diffusion coefficient of the CH equa-

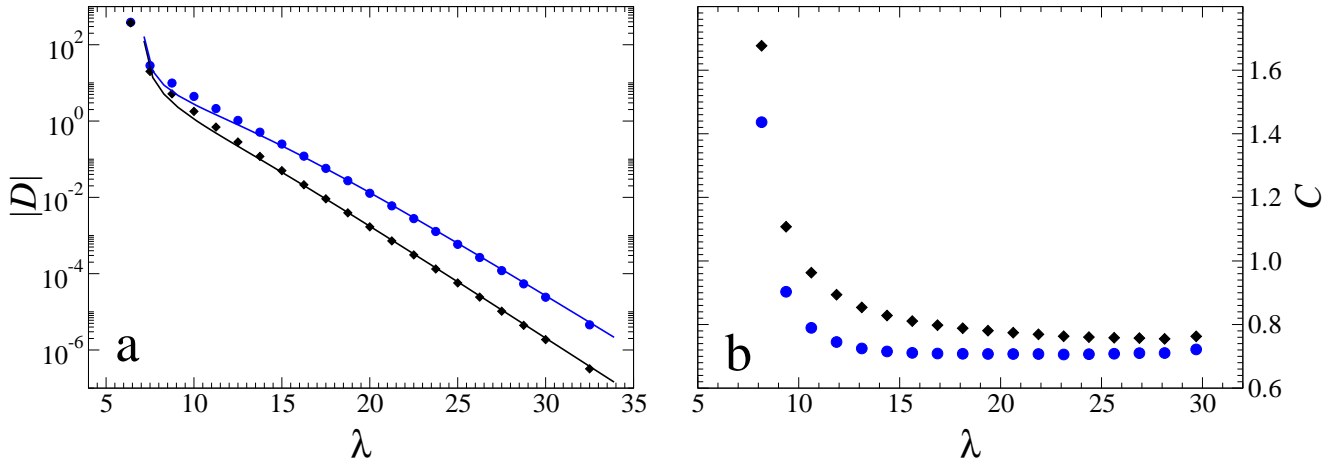


FIG. 4: (a) Phase diffusion coefficient D estimated with reduced expressions (14) and (15) for the Ginzburg-Landau equation (4a) (blue circles) and for the Cahn-Hilliard equation (5a) (black rhombi), respectively. Solid lines represent values of D calculated from Eqs. (33) and (34). Note that for these two cases D is negative until the sensibility of the algorithm (in this case of order 10^{-7}). The stationary solutions u_0 have been obtained with a mesh size $\Delta x = 0.025$, a varying time step Δt decreasing from 1 to 10^{-6} , and a maximum residue $\rho_m = 10^{-8}$. The q derivatives in (14) and (15) are estimated by evaluating four equally spaced u_0 around $q = 2\pi/\lambda$ with a $\Delta q = 2.5 \times 10^{-3}$. (b) Estimation of the coefficient C [$\lambda = C^{-1} \ln(t)$] for the Ginzburg-Landau equation (4a) (blue circles) and the Cahn-Hilliard equation (5a) (black rhombi). This coefficient is estimated through a linear regression of $\ln(|D|/\lambda^2)$ by applying a sliding window binning four consecutive values of $|D|$ from the left figure. The wavelength λ is the average of the different wavelengths of the points binned together. All units are arbitrary.

tion (5a) (the same for the α models). In the following, as an example, we detail how we have implemented the Newton-Raphson method to find the stationary solutions of the conserved Kuramoto-Sivashinsky equation.

The dynamic evolution of the cKS equation presents several numerical difficulties, which can be ascribed to the nature of its stationary solutions: a sequence of arcs of parabola whose amplitude grows quadratically with λ , while their joining regions have a diverging curvature and a vanishing size [8, 11]. This leads to the blow up of the integration scheme for large time steps. More specifically, the numerical integration of a system with $\Delta x = 0.1$ and $N = 2048$, i.e., $L = 204.8$, must be performed with our IFABM4 code by choosing $\Delta t = 10^{-5}$ in order to prevent the blow up at $t_{max} \sim 10^3$. For this reason, the phase diffusion method is very suitable to estimate numerically the coarsening law for the cKS equation. In this case, instead of performing a first estimation of the stationary solutions u_0 by means of the pseudospectral algorithm, we have solved directly the equation

$$(1 - \tau q \partial_\phi + q^2 \partial_\phi^2) u - q^2 (\partial_\phi u)^2 = 0, \quad (23)$$

by discretizing the differential operators with sixth-order centered finite differences. In this way Eq. (23) is transformed in a set of N nonlinear equations in the space of the variables u_i (with $i = 1, \dots, N$) that is solved by finding the zeros of the set of functions

$$F_i = u_i + q^2 B_i - q A_i (\tau + q A_i), \quad (24)$$

where A_i, B_i are given by

$$A_i = (\partial_\phi u)_i = \frac{1}{\Delta \phi} \sum_{j=1}^3 a_j (u_{i+j} - u_{i-j}), \quad (25)$$

$$B_i = (\partial_\phi^2 u)_i = \frac{1}{\Delta \phi^2} \left[b_0 u_i + \sum_{j=1}^3 b_j (u_{i+j} + u_{i-j}) \right], \quad (26)$$

and the coefficients a_j, b_j are listed in Table I. These vectors are built by taking into account the periodic boundary conditions of u_i . The Jacobian J of this system of equation is needed in order to solve the problem. The elements of this matrix are $J_{i,j} = \partial_{u_j} F_i$, which is a band matrix with

$$J_{i,i} = 1 + \frac{q^2 b_0}{(\Delta \phi)^2}, \quad (27)$$

$$J_{i,i \pm j} = (\Delta \phi)^{-2} [q^2 b_j \mp q a_j (\tau \Delta \phi + 2q A_i)],$$

where $j = 1, 2, 3$. Through the Matlab[®] function `fsolve`, the values of u_i for which $F_i = 0$ are readily found by means of the standard large-scale method implemented in the package, i.e., the `trust-region-reflective` algorithm (for details see Refs. [22, 23] and the Matlab[®] documentation). Some stationary solutions u_0 of the cKS equation for $\tau = 0$ are reported in Fig. 2(a).

To conclude this section we present one case in which the Newton-Raphson method has been used to decrease the residue of the stationary solution found by our IFABM4 code. As working example we consider the non-conserved α model (4b) with $\alpha = 2$. In Fig. 3 we show

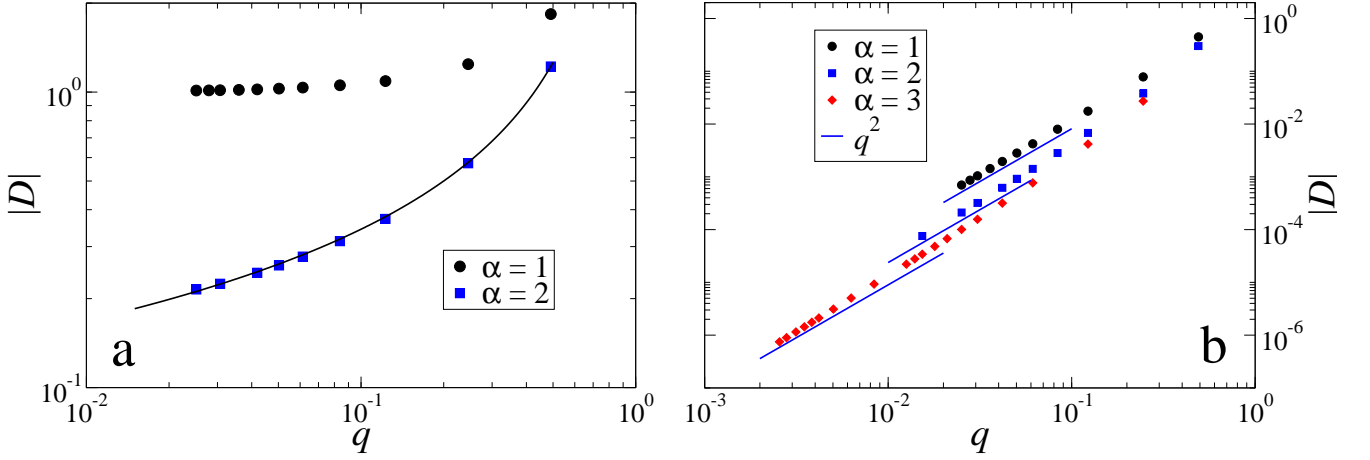


FIG. 5: (a) Modulus of the phase diffusion coefficient of the non-conserved α models (4b) for different values of the parameter α . The stationary solutions have been obtained through two steps: (i) a first approximation of u_0 is obtained by employing the IFABM4 algorithm up to a precision of about $\rho_m \sim 10^{-7}$, (ii) the final value of the stationary solution is found by refining the result of the previous step through the Newton-Raphson method. We used a spatial discretization $\Delta\phi = 0.025$ and $\Delta q = 1.0 \times 10^{-4}$ for $\alpha = 1, 2$, whereas $\Delta\phi = 0.05$ and two different $\Delta q = 1.0 \times 10^{-4}, 2.5 \times 10^{-5}$ ensuring a ratio $\Delta q/q < 10^{-2}$ for the case $\alpha = 3$ (see right figure). The coefficient D has been estimated through Eq. (14). According to previous analytical calculations [1] its asymptotic value saturates to a constant value, i.e., $|D| \sim 1$, when $\alpha \leq 2$. The solid line is a fit $|D| = a_0/(a_1 + \ln(q))$, showing the logarithmic correction for $\alpha = 2$. (b) Estimation of $|D|$ by means of (15) for the conserved α models (5b) with $\alpha = 1, 2, 3$. We used the same stationary solutions found for the non-conserved α models. The expected power law for these conserved models is $|D| \sim q^2$ [1]. The blue solid lines are guides to eyes with slope equal to two. All units are arbitrary.

the solution u_0 (black line) and the residue $\rho(\phi)$ before (blue, thin line) and after (red, dashed line) the NR minimization. The residues of the starting guess (blue line) had $\rho_\infty = 2.14 \times 10^{-9}$ and $\rho_2 = 1.35 \times 10^{-10}$, but, after the minimization step, these residues reduced to $\rho_\infty = 1.34 \times 10^{-9}$ and $\rho_2 = 1.12 \times 10^{-11}$. Note the drastic reduction of $\rho(\phi)$ in the regions characterized by small values of $\partial_\phi u_0$ leading to a ρ_2 that is one order of magnitude smaller than before the Newton-Raphson minimization.

index i	0	1	2	3	4
a_i	-	3/4	-3/20	1/60	-
b_i	-49/18	3/2	-3/20	1/90	-
c_i	-	-61/30	169/120	-3/10	7/240
d_i	91/8	-122/15	169/60	-2/5	7/240

TABLE I: Coefficients of the sixth-order finite difference discretization of the differential operators used in the Newton-Raphson minimization.

B. Solution of the adjoint operator and calculation of D

The solution of the adjoint problem $\mathcal{L}_0^\dagger[v] = 0$ is easily found through the finite difference discretization introduced in the previous section. Again, let us consider the conserved Kuramoto-Sivashinsky equation. Taking into

account that in Eq. (19) we have derivatives up to fourth order, first and second derivatives are discretized according to Eqs. (25) and (26), and third and fourth derivatives are given by

$$(\partial_\phi^3 v)_i = (\Delta\phi)^{-3} \sum_{j=1}^4 c_j (v_{i+j} - v_{i-j}), \quad (28)$$

$$(\partial_\phi^4 v)_i = (\Delta\phi)^{-4} \left[d_0 v_i + \sum_{j=1}^4 d_j (v_{i+j} + v_{i-j}) \right], \quad (29)$$

where the coefficients c_j and d_j are listed in Table I.

The derivatives $\partial_\phi^2 u_0$ and $\partial_\phi u_0$ are computed in Fourier space. The elements of these vectors multiply the constant coefficient of the finite difference discretization of the differential operators of Eq. (19), thus forming the sparse matrix M , which represent the discrete version of Eq. (19). Then, by means of the Matlab[®] function `eigs` (that is based on the Fortran library `ARPACK`), we search for the eigenvalues of M , which are in modulus closer to zero and their associated eigenvectors. The eigenvector \hat{v} related to the smallest eigenvalue is finally normalized in order to have a solution v_0 with zero mean and amplitude equal to one

$$v_0 = \frac{\hat{v} - \langle \hat{v} \rangle}{\max(|\hat{v}|)}. \quad (30)$$

Some functions v_0 for the cKS equation for $\tau = 0$ are reported in Fig. 2(b).

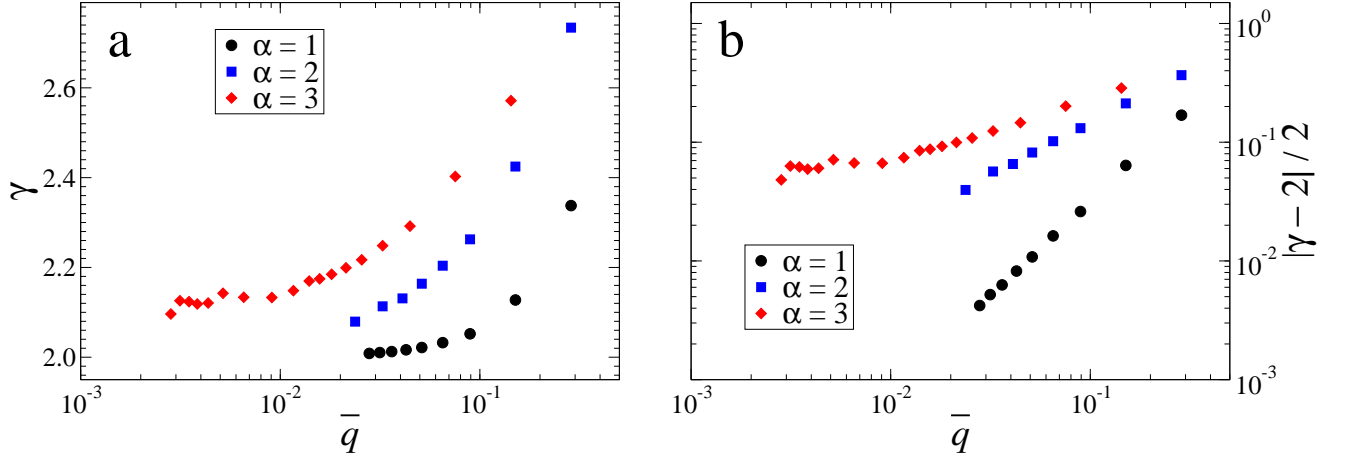


FIG. 6: (a) Estimation of the power-law behavior of the absolute value of the phase diffusion coefficient of the conserved α models for different values of α . The exponent γ (that is $|D| \sim q^\gamma$) is computed by a linear regression of three consecutive points of each curve of Fig. 5(b). The center of the sliding window \bar{q} is the mean value of the abscissa of these points. (b) Relative error of the estimated exponent γ as function of the mean value of the window position \bar{q} . Note the different convergence rate for every α . All units are arbitrary.

The values of the phase diffusion coefficient D are computed according to Eqs. (14), (15), and (20). As for the solution of the adjoint operator, in these equations ϕ derivatives are calculated through Fourier differentiation, whereas q derivatives are discretized by a fourth-order centered finite differences, i.e.,

$$\partial_q u_0(q) = \frac{1}{12\Delta q} \left[-u_0(q + 2\Delta q) + 8u_0(q + \Delta q) - 8u_0(q - \Delta q) + u_0(q - 2\Delta q) \right]. \quad (31)$$

These four additional stationary solutions, which are equally distributed around $u_0(\phi; q)$ and separated by a factor Δq , are found by keeping constant the number of discretization points but changing the length of the system λ , that is $2\pi/q$. In this manner we are able to directly compare the values of these four functions and readily obtain the discrete representation of $\partial_q u_0(\phi; q)$. The integrals involved in the calculation of D are evaluated numerically by the extended Simpson's rule [19].

The functional relation between the phase diffusion coefficient and the wavelength is found by computing D at discrete increasing system size (keeping constant the spatial discretization in ϕ space). After the estimation of D for a given q_1 , the stationary solution for $q_2 < q_1$ is computed by using the information provided by $u_0(q_1)$. The starting guess we used to determine $u_0(q_2)$ was a vector of $N_2 = 2\pi/q_2\Delta\phi$ Fourier modes formed by the Fourier transform of $u_0(q_1)$ for the first $N_1 = 2\pi/q_1\Delta\phi$ elements and zero padded for the others $N_2 - N_1$. Moreover, the amplitude of this initial guess has been adjusted according to the previously observed solutions. In fact, during the estimation of u_0 for decreasing values of q , we record the amplitude of these solutions and we are able to forecast the amplitude of the successive stationary solution (at least roughly). In this manner we are able to reduce

the computational cost needed to estimate the new value of D . Finally, after the estimation of D for a set of increasing wavelength, the coarsening law follows by the inversion of relation (13), which leads to $L(t) \sim \sqrt{|D(L)|t}$.

IV. RESULTS

We now report and discuss the results we obtained using the numerical methods described in previous sections. Let us start with the simplest and well known models: the GL model (4a) and its conserved version, the CH model (5a). They admit analytical solutions based on the Jacobi elliptic function $\text{Sn}(x; p)$ [24], allowing us to test our numerical procedure with a controlled result. This family of solution is parametrized by the elliptic modulus $p \in [0, 1]$ (for more details see Appendix B) and take the form

$$u_0(x) = A \text{Sn} \left(\frac{4K}{\lambda} x; p \right). \quad (32)$$

The dependence of the complete elliptic integral of the first kind K and the amplitude A on the elliptic modulus p is reported in Appendix B, Eqs. (17) and (18), respectively. It has already been shown that for these two models the value of the phase-diffusion coefficient can be expressed as a function of λ , the amplitude of u_0 and the integrals $J = \int_0^\lambda (u'_0)^2 dx$ for the GL model or $I = \int_0^\lambda u_0^2 dx$ for its conserved counterpart [1, 3]

$$D = -\frac{\lambda^2(A - A^3)}{J \partial_A \lambda} \quad \text{GL equation}, \quad (33)$$

$$D = -\frac{\lambda^2(A - A^3)}{I \partial_A \lambda} \quad \text{CH equation}. \quad (34)$$

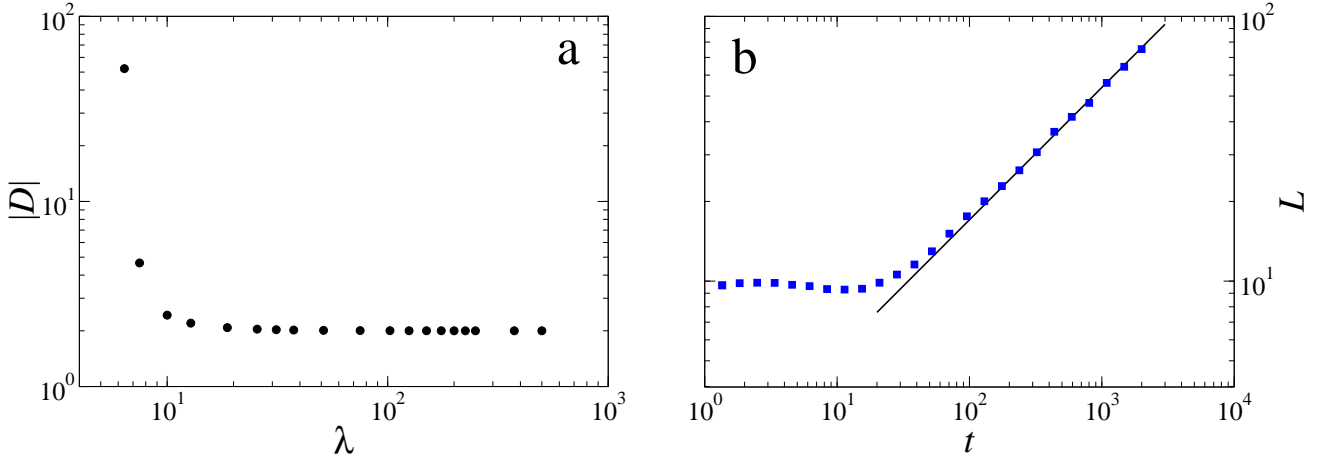


FIG. 7: (a) Absolute value of the phase diffusion coefficient D of the cKS equation (6) in the case of $\tau = 0$ for different values of λ . We have used a fixed mesh discretization $\Delta\phi = 0.025$ and a variable q discretization $\Delta q = 1.0 \times 10^{-3}, 2.5 \times 10^{-4}, 1.0 \times 10^{-4}$ ensuring a ratio $\Delta q/q < 10^{-2}$ for the different values of λ . (b) Dynamical evolution of Eq. (6) for $\tau = 0$ with simulation parameters $N = 2048$, $\Delta\phi = 0.1$, and $\Delta t = 10^{-5}$. The values of λ are averaged over 50 different random initial conditions whose elements are sampled from a Gaussian distribution with zero mean and unit variance. The black solid line is a guide to eyes with slope $1/2$. All units are arbitrary.

As depicted in Appendix B, we can compute all these functions and their derivatives with respect to A through complete elliptic integrals of first or second kind and Jacobi elliptic functions. Finally, the integrals I and J are easily evaluated by means of adaptive quadrature so that the values of D are obtained without solving any differential equation.

In the absence of noise, the Ginzburg-Landau and the Cahn-Hilliard model display a logarithmic coarsening, $L(t) \simeq C^{-1} \ln t$, which corresponds, in the formalism of phase diffusion equation, to a diffusion coefficient which decreases exponentially with the wavelength of the stationary solution, $D(\lambda) \simeq e^{-C\lambda}$. Figure 4(a) shows such exponential behavior on a lin-log scale while Fig. 4(b) shows the convergence of the constant C to a value of order 0.75 for both models. Note that in Fig. 4(a) the comparison between the values of D estimated numerically (symbols) and those obtained through Eqs. (33) and (34) (lines) confirms the validity of our method in a well-controlled situation and its applicability to other non-trivial cases.

Next, we consider the nonconserved and conserved α models, given by Eqs. (4b) and (5b), respectively. According to the analytic treatment of the phase diffusion equation [1] and to numerics (taking care of dangerous caveats [25]), we expect that the coarsening exponent for the nonconserved models is $n = 1/2$ for $1 \leq \alpha < 2$ and $n = \alpha/(3\alpha - 2)$ for $\alpha > 2$. Case $\alpha = 2$ has a logarithmic correction, $L(t) \simeq \sqrt{t}/\ln t$. Conserved models, instead show a constant coarsening exponent, $n = 1/4$, for all α . Figure 5(a) considers cases $\alpha = 1, 2$ for non-conserved models, therefore we expect a constant D for $\alpha = 1$ and $D \approx 1/\ln q$ for $\alpha = 2$. This is exactly what our numerics shows. In Fig. 5(b) we consider $\alpha = 1, 2, 3$

for the conserved models and, as expected, $|D| \simeq q^2$ for small q . The conserved case is analyzed in more details in Figs. 6(a) and 6(b). On the left we plot the exponent γ defined by $|D| \simeq q^\gamma$, and on the right we specialize on its convergence to the asymptotic value $\gamma_\infty = 2$. According to the results displayed in Fig. 6(b), for a larger exponent α we observe a slower convergence to the asymptotic γ_∞ . This effect is more pronounced for the case $\alpha = 3$ where a crossover region between two power laws has been already reported in Ref. [25]. Taking into account that this region is of the order $\lambda \sim 10^3$, i.e., $q \sim 0.006$, and for this wavelength our algorithm estimates a $|D|$ smaller than 10^{-5} , it is difficult to assess a clear asymptotic value for γ and the relative error $|\gamma - \gamma_\infty|/\gamma_\infty$ saturates to a value around 5%.

In Figs. 7(a) and 7(b) we consider the cKS model (6). Some numerical and approximated analytical estimations of the coarsening exponents gave $n = 1/2$, i.e., a constant phase diffusion coefficient. This is shown on the left, while the right shows a clear evaluation of the coarsening exponent through the direct integration of the dynamical equation. Our results are much cleaner than available results in the literature.

Finally we compare the computational cost used to estimate the coarsening exponent by means of the phase diffusion method with the cost of the standard method used in the literature, that is, typically, the direct integration of the time-dependent PDE. We consider three cases of conserved models that are usually stiffer than their non-conserved counterparts due to high-order spatial derivatives. Lines in Fig. 8 are found after the inversion of the relation $\lambda^2/|D| \sim t$ that leads to the coarsening law $L(t) \sim t^n$. In the same figure, symbols are data obtained from the numerical integration of time-

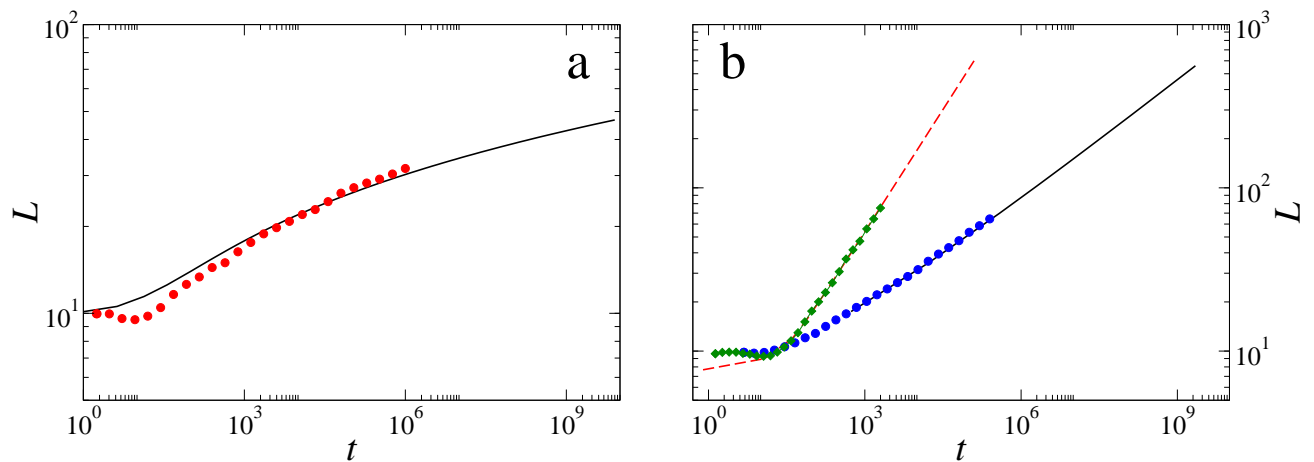


FIG. 8: Comparison between the phase diffusion method and the numerical integration of the time-dependent PDE for three different models. (a) Case of logarithmic coarsening, the Cahn-Hilliard equation. The black line is the estimation of λ as function of t from the data displayed in Fig. 4(a). The red circles are the numerical integration of Eq. (5a) by means of our IFABM4 code with parameters $L = 102.4$, $\Delta x = 0.1$, $\Delta t = 0.05$, and averaged over 50 different initial conditions (generated from a normal distribution with zero mean and unit variance). (b) Case of power-law coarsening. As for the left panel, lines stand for the estimation of λ as function of t from the values of $D(\lambda)$ while the symbols are obtained from the numerical integration of time dependent equations. The black solid line [from data in Fig. 5(b)] and the blue circles are data for the conserved α model Eq. (5b) with $\alpha = 2$ and parameters $L = 256$, $\Delta x = 0.25$, $\Delta t = 0.05$, and averaged over 50 different initial conditions. The red dashed line and the green rhombi correspond to the conserved Kuramoto-Sivashinsky equation (6). These data are computed (line) and reported (rhombi) from the left and the right panel of Fig. 7, respectively. All units are arbitrary.

dependent PDEs averaged over several realizations of different initial conditions (see captions for more details). As shown in the figure, the phase diffusion method allows one to extract the coarsening law for times that are orders of magnitude larger compared to the standard method. Moreover, the times listed in Table II demonstrate the remarkable performance of our implementation of the phase diffusion method. Note that in the three cases we have not employed the same strategy to find the stationary solutions of the different PDEs. As already explained in the previous sections, for the Cahn-Hilliard model we have only used our IFABM4 code with variable time stepping, for the conserved Kuramoto-Sivashinsky equation we have solved directly Eq. (23) with the Newton-Raphson method, and for the conserved α model we combined these two methods. We have also verified that the solution of the adjoint problem (19) for the cKS model is much less costly (roughly two orders of magnitude) than the determination of u_0 .

V. CONCLUSIONS

In this work we have demonstrated that the phase diffusion method can be a reliable and fast approach to find the coarsening law of nonlinear 1D partial differential equations. Its numerical implementation is straightforward and extends the applicability of the method beyond the cases studied in Ref. [1]. In fact, all these cases allowed an analytical evaluation of $L(t)$, which is not al-

ways possible (see the cKS equation).

Our algorithm permits us to evaluate the coarsening exponent with a negligible computational cost compared to standard methods, such as the direct numerical solution of the time-dependent PDE (see Table 2). Furthermore, it does not suffer from spurious effects associated with the finite size of the system or from errors arising in the time discretization of the PDE, and the result does not need to be averaged over several initial conditions.

The main limitation of the method is the finite accuracy in the estimation of D , which should be improved for larger times, when coarsening is slow (logarithmically slow or following a power law with a small exponent n). However, in such cases the direct time integration would require to attain extremely large times. Our discussion and in particular Table 2 shows that the phase diffusion method is computationally much faster than time integration.

A separate comment should be made for PDEs whose steady solutions are determined by an ODE of higher order than two. In these cases [26], which include the Swift-Hohenberg equation, we expect more branches of stationary solutions, $\lambda_i(A)$, which makes our analysis more complicated.

Finally, in this paper we confined our discussion to one-dimensional PDEs, but we have recently shown [27] that the phase diffusion method can be successfully applied to coarsening processes in two dimensions as well. It will be interesting to extend our numerical approach to the bidimensional case, especially for studying those equations that can hardly be attacked analytically.

	Phase diffusion (long time)	Integration (short time)	Integration (long time)	Ratio (long time) Integration/Phase diffusion
CH	8.32×10^2	8.54×10^4	$\sim 4.21 \times 10^9$	$\sim 5 \times 10^6$
c α -model ($\alpha=2$)	1.66×10^3	3.95×10^4	$\sim 7.41 \times 10^9$	$\sim 4 \times 10^6$
cKS	6.07×10^2	1.46×10^6	$\sim 1.47 \times 10^9$	$\sim 2 \times 10^6$

TABLE II: Actual computational time (in seconds) required to measure the coarsening exponent n with the phase diffusion method (second column) and with the numerical integration of the time-dependent PDE (third column). The fourth column is an estimation of the computational cost needed by the standard method to reach the same time span of the phase diffusion method for the data reported in Fig. 8. The fifth column is the ratio between the estimated time for the standard method and the cost for the phase diffusion method. The numerical experiments were carried out in a machine equipped with a single-processor Intel[®] Core[™] 2 Duo with a clock frequency of 2.4 Ghz.

Acknowledgements

M. N. and P. P. acknowledge support from the Italian Ministry of Research (PRIN 2007JHLPEZ). M. N. also acknowledges partial support by MICINN (Spain)

Grant No. FIS2009-12964-C05-01. C. M. acknowledges financial support from CNES (Centre National d'Etudes Spatiales) and thanks the Italian CNR for support from their International Exchange Program.

Appendix A: Pseudospectral algorithm

The solution of the linear part of Eq. (21) suggests the following change of variable

$$z_k(t) = e^{-\omega_k t} u_k(t), \quad (\text{A1})$$

and the temporal evolution of this new variable depends only on the nonlinear operator

$$\partial_t z_k(t) = e^{-\omega_k t} N[u(t)]_k. \quad (\text{A2})$$

This is our starting point to discretize Eq. (A2) in the time domain by using one of the standard algorithms available in the literature. In order to enhance the stability properties of our method we have chosen a fourth order predictor-corrector method, the Adams-Bashforth-Moulton (IFABM4) scheme. The predictor step applied to Eq. (A2) is

$$\begin{aligned} z_k(t + \Delta t) = z_k(t) + \frac{\Delta t}{24} \Big[& 55e^{-\omega_k t} N[u(t)]_k - 59e^{-\omega_k(t-\Delta t)} N[u(t-\Delta t)]_k \\ & + 37e^{-\omega_k(t-2\Delta t)} N[u(t-2\Delta t)]_k - 9e^{-\omega_k(t-3\Delta t)} N[u(t-3\Delta t)]_k \Big], \end{aligned} \quad (\text{A3})$$

that leads to a prediction for \bar{u}_k at the next time step

$$\bar{u}_k(t + \Delta t) = e^{\omega_k \Delta t} \left[u_k(t) + \frac{\Delta t}{24} (55N_0 - 59N_1 + 37N_2 - 9N_3) \right], \quad (\text{A4})$$

where the functions $N_n = e^{n\omega_k \Delta t} N[u_k(t - n\Delta t)]_k$ are computed during the time stepping of the algorithm by successive multiplications of the factor $\exp(\omega_k \Delta t)$. As before, the corrector step is applied to the variable $z_k(t + \Delta t)$ and is computed from the value of the predictor and the value of u_k at three previous time steps

$$\begin{aligned} z_k(t + \Delta t) = z_k(t) + \frac{\Delta t}{24} \Big[& 9e^{-\omega_k(t+\Delta t)} N[\bar{u}(t + \Delta t)]_k + 19e^{-\omega_k t} N[u(t)]_k \\ & - 5e^{-\omega_k(t-\Delta t)} N[u(t-\Delta t)]_k + e^{-\omega_k(t-2\Delta t)} N[u(t-2\Delta t)]_k \Big], \end{aligned} \quad (\text{A5})$$

so that the update of u_k reads

$$u_k(t + \Delta t) = \frac{3}{8} \Delta t N[\bar{u}(t + \Delta t)]_k + e^{\omega_k \Delta t} \left[u_k(t) + \frac{\Delta t}{24} (19N_0 - 5N_1 + N_2) \right]. \quad (\text{A6})$$

Equations (A4) and (A6) depend on four previous values of the function u_k , we have to compute the four initial time steps of the evolution of (21) by an integrator of the same accuracy, for example a classical fourth order Runge-Kutta method (RK4). For the variable z_k the RK4 method reads

$$z_k(t + \Delta t) = z_k(t) + \frac{\Delta t}{6} (f_1 + 2f_2 + 2f_3 + f_4), \quad (\text{A7})$$

where the different RK4 steps are obtained through a sequence of new variables. The first point in the RK4 evolution is easily found by evaluating Eq. (A2) at time t with the variable $u_k(t)$

$$f_1 = e^{-\omega_k t} \mathcal{N} \left[\mathcal{F}^{-1} \left[e^{\omega_k t} z_k(t) \right]_{\phi} \right]_k = e^{-\omega_k t} \mathcal{N}_0. \quad (\text{A8})$$

Then we introduce the new variable u_{1k} and we find the second RK4 point f_2

$$u_1 = \mathcal{F}^{-1} \left[e^{\omega_k \Delta t/2} \left(u_k(t) + \frac{\Delta t}{2} \mathcal{N}_0 \right) \right]_{\phi}, \quad (\text{A9})$$

hence $f_2 = \exp[-\omega_k(t + \Delta t/2)] \mathcal{N}[u_1]_k$. The same procedure is iterated, so that

$$u_2 = \mathcal{F}^{-1} \left[e^{\omega_k \Delta t/2} \left(u_k(t) + \frac{\Delta t}{2} \mathcal{N}[u_1]_k \right) \right]_{\phi}, \quad (\text{A10})$$

so that $f_3 = \exp[-\omega_k(t + \Delta t/2)] \mathcal{N}[u_2]_k$, and

$$u_3 = \mathcal{F}^{-1} \left[e^{\omega_k \Delta t} (u_k(t) + \Delta t \mathcal{N}[u_2]_k) \right]_{\phi}, \quad (\text{A11})$$

hence $f_4 = \exp[-\omega_k(t + \Delta t)] \mathcal{N}[u_3]_k$. Finally, the update for u_k reads

$$u_k(t + \Delta t) = e^{\omega_k \Delta t} \left[u_k(t) + \frac{\Delta t}{6} \mathcal{N}_0 \right] + \frac{\Delta t}{6} \left[2e^{\omega_k \Delta t/2} (\mathcal{N}[u_1]_k + \mathcal{N}[u_2]_k) + \mathcal{N}[u_3]_k \right]. \quad (\text{A12})$$

This last equation is used to warm up the predictor-corrector method with the three initial time steps.

Appendix B: Analytical solutions of the Ginzburg-Landau equation

The stationary states of the Ginzburg-Landau equation can be expressed analytically by means of the Jacobi elliptic function sine-amplitude $\text{Sn}(x; p)$ [24]. This family of solutions is parametrized by the elliptic modulus $p \in [0, 1]$ and take the form

$$u_0(x) = \sqrt{\frac{2p^2}{p^2 + 1}} \text{Sn} \left(\frac{x}{\sqrt{p^2 + 1}}; p \right), \quad (\text{B1})$$

and its derivative reads

$$u'_0(x) = \frac{\sqrt{2}p^2}{p^2 + 1} \text{Cn} \left(\frac{x}{\sqrt{p^2 + 1}}; p \right) \text{Dn} \left(\frac{x}{\sqrt{p^2 + 1}}; p \right), \quad (\text{B2})$$

where Cn and Dn are the other two Jacobi elliptic functions [28]. The periodicity of these functions is

$$\lambda = 4K(p)\sqrt{p^2 + 1}, \quad (\text{B3})$$

where the complete elliptic integral of the first kind is defined according to

$$K(p) = \int_0^1 \frac{dt}{\sqrt{(1-t^2)[1-p^2 t^2]}}. \quad (\text{B4})$$

Taking into account that the function $\text{Sn} \in [-1, 1]$, the amplitude of u_0 is a function of the elliptic modulus

$$A = \sqrt{\frac{2p^2}{p^2 + 1}}, \quad (\text{B5})$$

so that we are able to express the periodicity of the stationary solution as a function of its amplitude

$$\lambda(A) = 4\sqrt{\frac{2}{2-A^2}} K\left(\frac{A}{\sqrt{2-A^2}}\right). \quad (\text{B6})$$

The variation of λ with respect to the amplitude of u_0 is

$$\partial_A \lambda = \frac{4}{A} \left(\frac{2}{2-A^2}\right)^{1/2} \left[\frac{1}{1-A^2} E\left(\frac{A}{\sqrt{2-A^2}}\right) - K\left(\frac{A}{\sqrt{2-A^2}}\right) \right], \quad (\text{B7})$$

where the complete elliptic integral of the second kind is

$$E(p) = \int_0^1 dt \sqrt{\frac{1-p^2 t^2}{1-t^2}}. \quad (\text{B8})$$

-
- [1] P. Politi, and C. Misbah, Nonlinear dynamics in one dimension: A criterion for coarsening and its temporal law, *Phys. Rev. E* **73**, 036133 (2006).
 - [2] Coarsening may also occur when there is a minimal wave vector q_{min} below which $\omega(0) < 0$ as in Ref. [29]. However, this scenario is out of our interest.
 - [3] P. Politi and C. Misbah, When Does Coarsening Occur in the Dynamics of One-Dimensional Fronts?, *Phys. Rev. Lett.* **92**, 090601 (2004).
 - [4] A negative D might imply an anticoarsening process as well, in principle. However, here we don't consider this scenario.
 - [5] A. J. Bray, Theory of phase-ordering kinetics, *Adv. Phys.* **43**, 357 (1994).
 - [6] P. Politi and J. Villain, Ehrlich-Schwoebel instability in molecular-beam epitaxy: A minimal model, *Phys. Rev. B* **54**, 5114 (1996).
 - [7] P. Politi and A. Torcini, Coarsening in surface growth models without slope selection, *J. Phys. A: Math. Gen.* **33**, L77 (2000).
 - [8] Z. Csahók, C. Misbah, F. Rioual, and A. Valance, Dynamics of aeolian sand ripples, *Eur. Phys. J. E* **3**, 71 (2000).
 - [9] F. Gillet, Z. Csahok, and C. Misbah, Continuum nonlinear surface evolution equation for conserved step-bunching dynamics, *Phys. Rev. B* **63**, 241401 (2001).
 - [10] T. Frisch and A. Verga, Effect of Step Stiffness and Diffusion Anisotropy on the Meandering of a Growing Vicinal Surface, *Phys. Rev. Lett.* **96**, 166104 (2006).
 - [11] P. Politi and D. ben-Avraham, From the conserved Kuramoto-Sivashinsky equation to a coalescing particles model, *Physica D* **238**, 156 (2009).
 - [12] R. Hoyle, *Pattern formation* (Cambridge University Press, Cambridge, 2006).
 - [13] D. Zwilling, *Handbook of differential equations* (Academic Press, San Diego, 1989)
 - [14] If $q = q(X, T)$ when deriving the phase diffusion equation, at the end (i.e., after taking derivatives) q is a constant, $q = 2\pi/\lambda$, because we are interested in the perturbation of a periodic solution, where q is constant.
 - [15] L. N. Trefethen, *Spectral Methods in MATLAB* (SIAM, Philadelphia, 2000).
 - [16] J. P. Boyd, *Chebyshev and Fourier Spectral Methods* (Dover, New York, 2001).
 - [17] B. Fornberg, *A Practical Guide to Pseudospectral Methods* (Cambridge University Press, Cambridge, 1996).
 - [18] C. Canuto, M. Y. Hussaini, A. Quarteroni, and T. A. Zhang, *Spectral Methods, Fundamentals in Single Domains* (Springer-Verlag, Berlin, 2006).
 - [19] W. H. Press, S. A. Teukolsky, W. T. Vetterling, and B. P. Flannery, *Numerical Recipes, The Art of Scientific Computing*, 3rd Ed. (Cambridge University Press, New York, 2007).
 - [20] A.-K. Kassam, and L. N. Trefethen, Fourth-Order Time-Stepping for Stiff PDEs, *SIAM J. Sci. Comput.* **26**, 1214 (2005).
 - [21] S. M. Cox, and P. C. Matthwes, Exponential Time Differencing for Stiff Systems, *J. Comput. Phys.* **176**, 430 (2001).
 - [22] T. F. Coleman, and Y. Li, On the Convergence of Reflective Newton Methods for Large-Scale Nonlinear Minimization Subject to Bounds, *Math. Program.* **67**, 189 (1994).
 - [23] T. F. Coleman, and Y. Li, An Interior, Trust Region Approach for Nonlinear Minimization Subject to Bounds, *SIAM J. Optimiz.* **6**, 418 (1996).
 - [24] S. Villain-Guillot, 1D Cahn-Hilliard dynamics: Ostwald ripening and application to modulated phase systems, *Phys. Lett. A* **372**, 7161 (2008).
 - [25] P. Politi and A. Torcini, Asymptotic and effective coarsening exponents in surface growth models, *Eur. Phys. J. B* **53**, 401 (2006).
 - [26] L. A. Peletier and W. C. Troy, *Spatial Patterns. Higher Order Models in Physics and Mechanics* (Birkhäuser, Boston, 2001).
 - [27] C. Misbah and P. Politi, Phase instability and coarsening in two dimensions, *Phys. Rev. E* **80**, R030106 (2009); S. Biagi, C. Misbah and P. Politi, Coarsening Scenarios in Unstable Crystal Growth, *Phys. Rev. Lett.* **109**, 096101 (2012).
 - [28] Eric W. Weisstein, *Jacobi Elliptic Function*. From MathWorld—A Wolfram Web Resource.

- <http://mathworld.wolfram.com/JacobiEllipticFunctions.html> a conservation law, *Nonlinearity* **13**, 1293 (2000).
- [29] P. C. Matthews and S. M. Cox, Pattern formation with